Supporting Information

Solution-processed SnO_2/SnS_2 bilayer-based robust memristors for reliable neuromorphic computing

Xiuyang Tang, Xinming Ma, Sizhu Ha, Weifang Sun, Niwei He, Song Xue, Gangri Cai and Jin Shi Zhao**

Tianjin Key Laboratory of Organic Solar Cells and Photochemical Conversion, Department of Applied Chemistry, State Key Laboratory of Crystal Materials, Tianjin Key Laboratory of Functional Crystal Materials, Institute of Functional Crystals, School of Integrated Circuit Science and Engineering, Tianjin University of Technology, No. 391 Binshui Xidao, Xiqing District Tianjin 300384, P. R. China.

E-mail: grcai@email.tjut.edu.cn; jinshi58@tjut.edu.cn

Detail Experiments

Device preparation: Devices were fabricated on indium tin oxide (ITO) conductive glass substrates (Guro Glass Co.). A 20% aqueous solution of ammonium sulfide ($(NH_4)_2S$, Mw = 68.14) was sourced from Aladdin Biochemical Technology Co., Ltd. (Shanghai), and tin disulfide (SnS_2, Mw = 182.83) powder for the dielectric layer was obtained from Sino-Nova New Materials (Beijing) Tech Co. The ITO substrates were cut into 2×1.5 cm pieces and sequentially sonicated in deionized water, acetone, and ethanol for 30 min each. After nitrogen drying, they were aged at room temperature for 24 h to ensure complete dryness, followed by a 30-min ozone treatment prior to dielectric layer deposition. The SnS_2 precursor solution was prepared by mixing 4 mL of $(NH_4)_2S$ solution with 0.182 g of SnS_2 powder, then heated and stirred at 50 °C for 24 h to yield a clear solution. The SnS2 film was spin-coated onto ITO substrates at 5000 rpm for 30 s and annealed at 300 °C for 30 min in an argon atmosphere with a 2 °C/min ramp rate. For the SnO_2 layer, 0.5025 g of $SnCl_2{\cdot}2H_2O$ and 0.335 g of thiourea (CH_4N_2S) were dissolved in 15 mL of deionized water, heated and stirred at 50 °C for 48 h in air. The resulting clear solution was spin-coated onto the annealed SnS_2 film, which was then annealed under identical argon conditions. The top ITO electrode was deposited by magnetron sputtering through a 150-μm aperture mask plate, with an O_2/Ar_2 flow ratio of 5.4 sccm:53.9 sccm, an 8 mTorr operating pressure, 80 W power, and 40 min deposition time.

Characterizations: Atomic force microscopy (AFM, Dimension Icon, Bruker AXS) characterized film morphologies. Visible-range (300-900 nm) transmission spectra were measured using a PerkinElmer Lambda 750 UV/VIS/NIR spectrometer. TEM samples

were prepared via focused ion beam (FIB) milling with a dual-beam system (FEI Helios Nanolab 460 HP), and high-resolution TEM (HRTEM) imaging was performed on an FEI Tecnai F200X at 200 kV. X-ray photoelectron spectroscopy (XPS, ESCALAB 250 XI, Thermo Scientific), X-ray diffraction (Ultima IV, Rigaku), and Raman spectroscopy (RENISHAW inVia, 532 nm, 20 mW, 100-800 cm^{-1}) analyzed material structures and compositions. Film surface features were examined by field emission scanning electron microscopy (FESEM, ZEISS MERLIN Compact).

Electrical properties were evaluated using a semiconductor parameter analyzer (Anjie B1500) integrated with an Agilent pulse generator. During testing, the top ITO electrode received voltage or pulse inputs while the bottom ITO was grounded. I-V characterization scans ranged from -4 V to 4 V. Durability was assessed by continuous DC scanning, and retention tests were conducted at room temperature and 85 °C, both using a 0.1-V reading voltage. Synaptic functions were investigated by applying diverse pulse voltages through a pulse module to mimic various synaptic behaviors.

Additional Figs

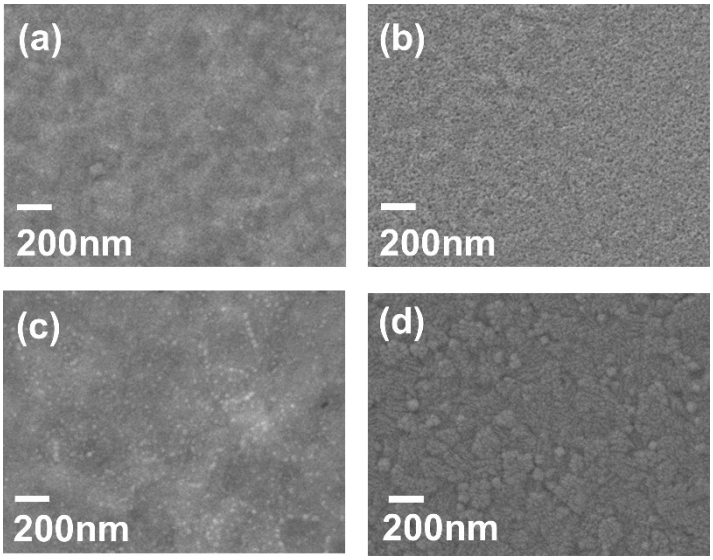

Fig S1. SEM images of (a) SnS_2/ITO, (b) SnO_2/ITO, (c) SnO_2/SnS_2/ITO and (d) ITO glass

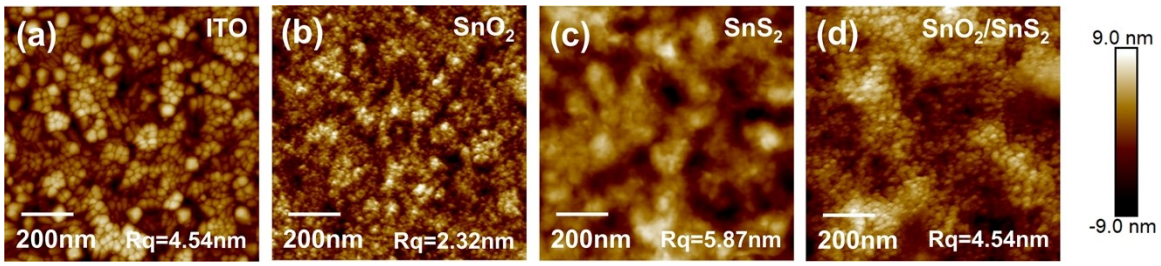

Fig S2. AFM images of (a) ITO, (b) SnO_2/ITO, (c) SnS_2/ITO, (d) SnO_2/SnS_2/ITO.

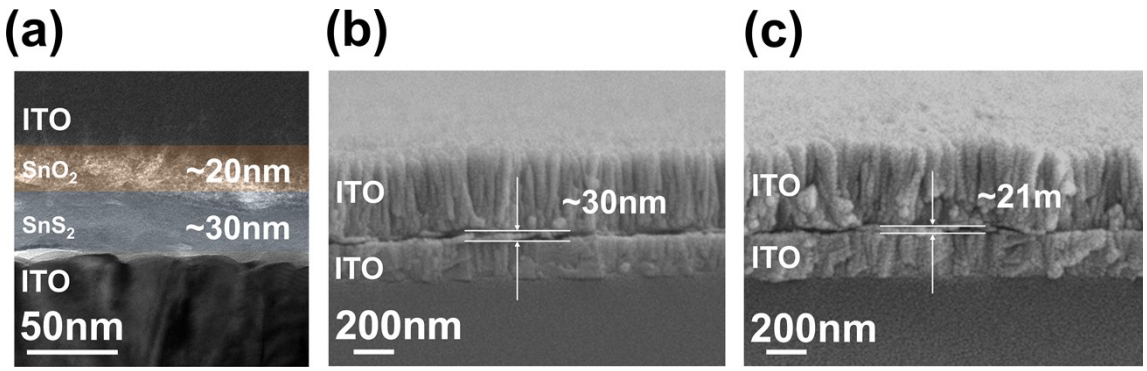

Fig S3. (a) HRTEM interface thickness image of OSM, FESEM cross-section images of (b) SM and (c) OM.

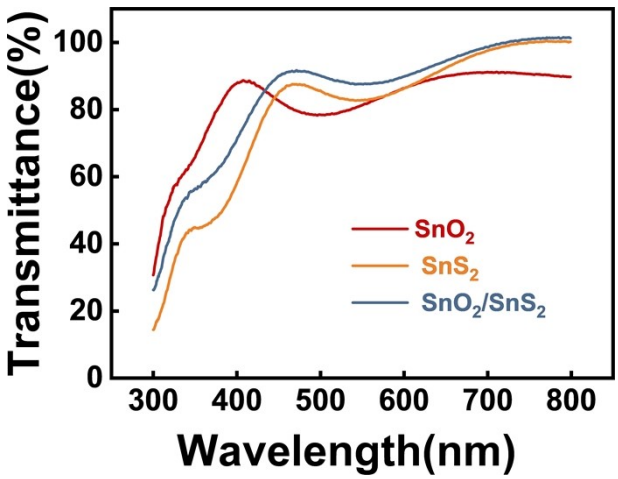

Fig S4. Uv-vis spectrum of the spin-coating deposited OM, SM, and OSM.

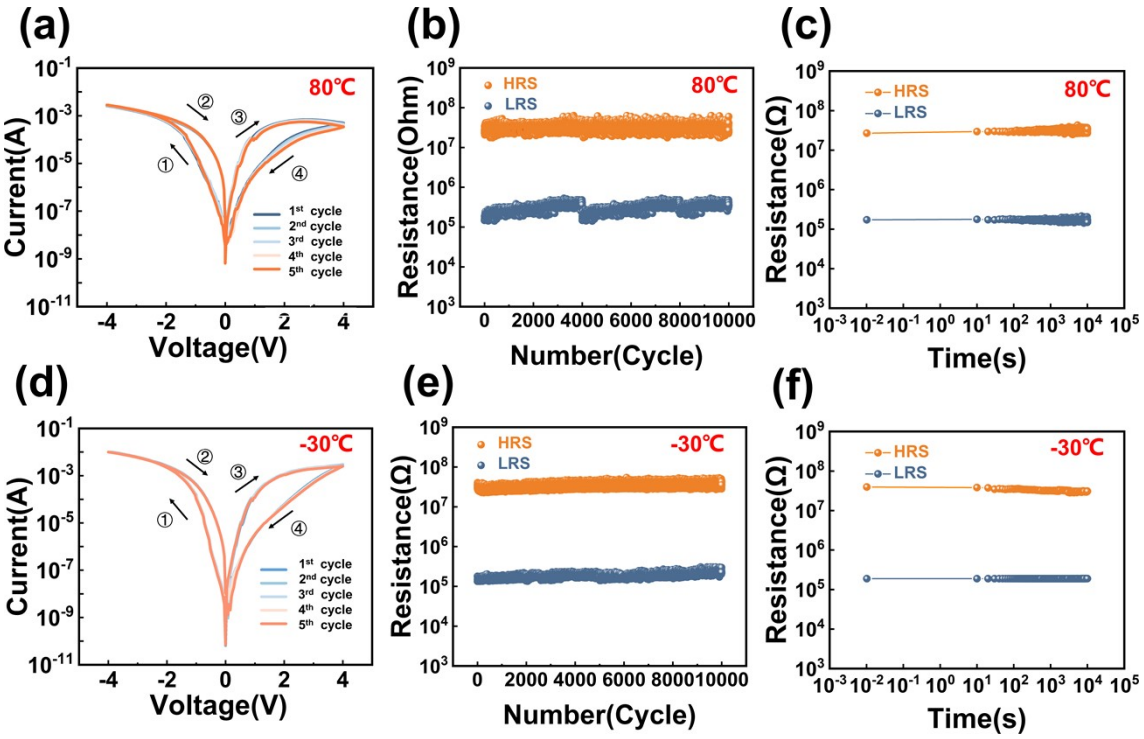

Fig S5. (a) The I-V of the OSM at 80℃. (b) The endurance of the OSM at 80℃. (c) The retention of the OSM at 80℃. (d) The I-V of the OSM at -30℃. (e) The endurance of the OSM at -30℃. (f) The retention of the OSM at-30℃.

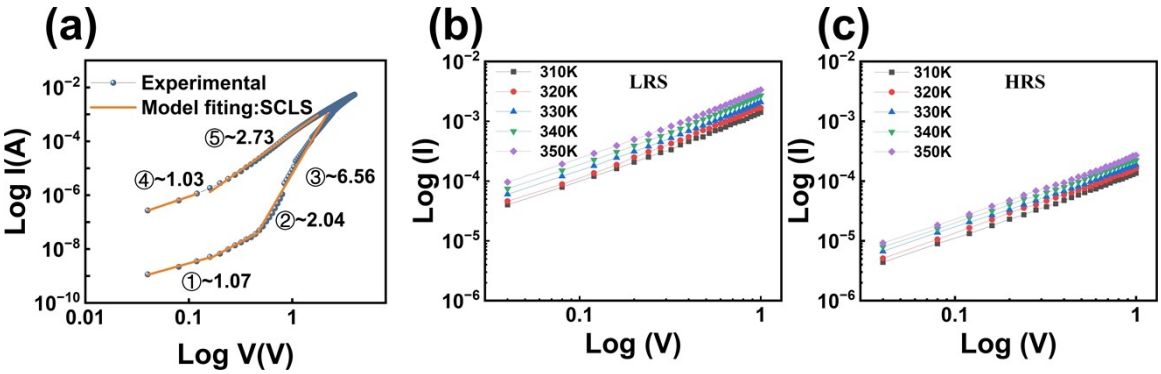

Fig S6. (a) The I-V data in double-logarithmic coordinates, the influence of temperature on (b) R_{LRS} and (c) R_{HRS} of the OSM.

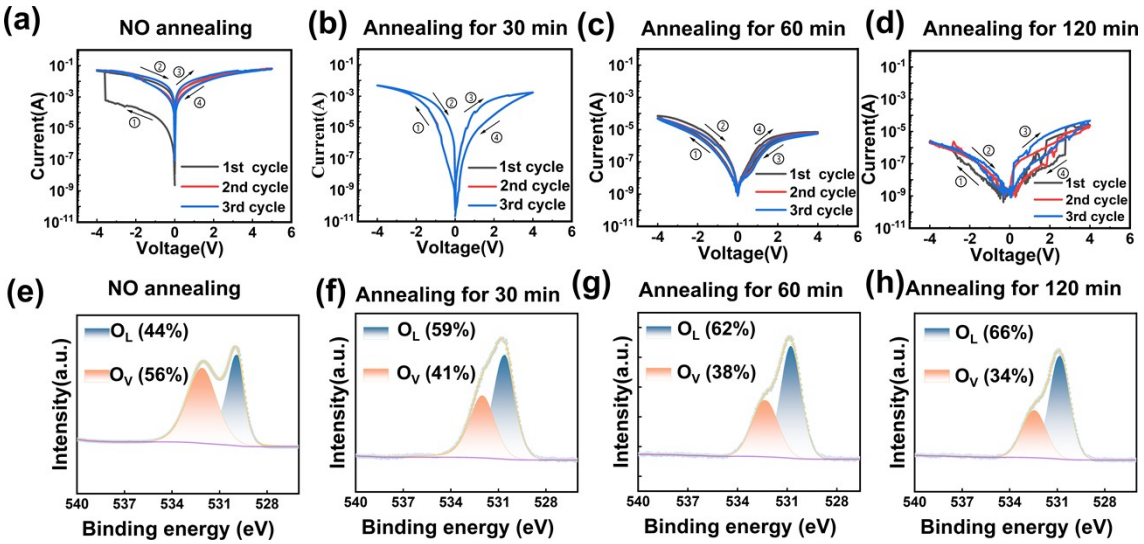

Fig S7. The I-V curves of OSMs: (a) unannealed, (b) annealed for 30 mins, (c) annealed for 600 mins, and (d) annealed for 120 mins; O 1s XPS spectrum of OSMs: (e) unannealed, (f) annealed for 30 mins, (g) annealed for 600 mins, and (h) annealed for 120 mins.

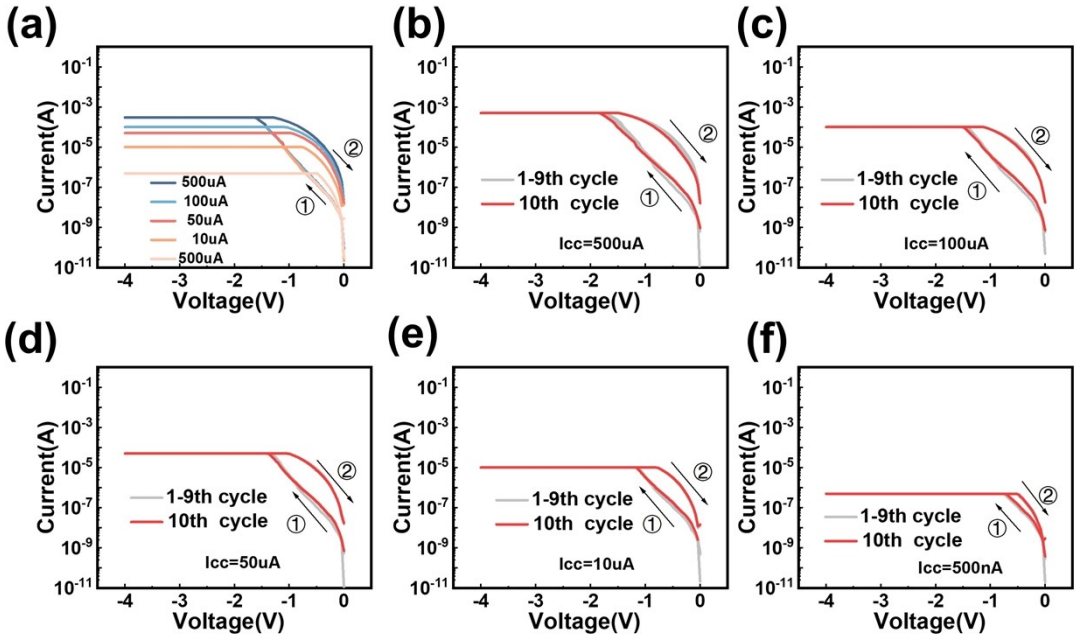

Fig S8. (a) The I-V diagrams of OSM with different current limiting conditions; 10 I-V cycles of OSM with different current limits: (b) 500 μA, (c) 100 μA, (d) 50 μA, (e) 10 μA, and (f) 500 nA.

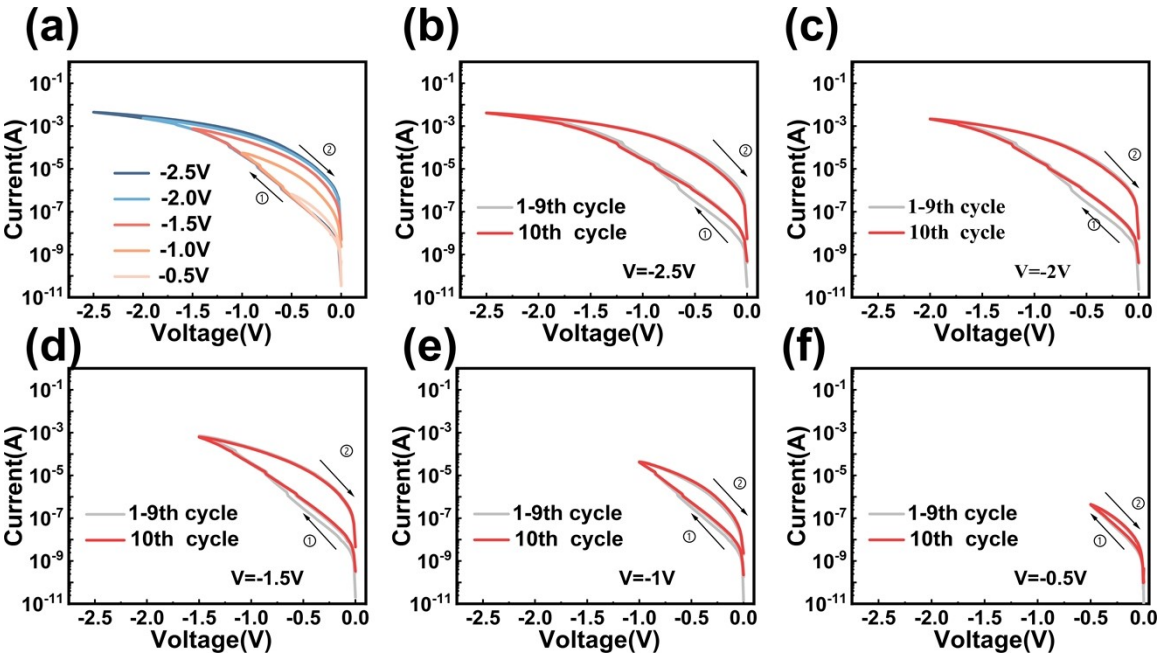

Fig S9. (a) The I-V diagrams of OSM under different set voltages; 10 I-V cycles of OSM at different set voltages: (b) -2.5 V, (c) -2 V, (d) -1.5 V, (e) -1 V, and (f) -0.5 V.

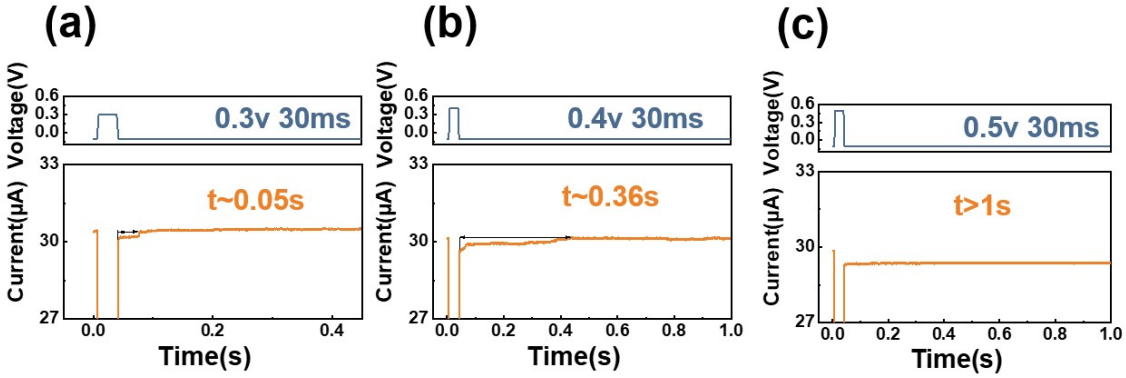

Fig S10. The EPSC dependence on pulse amplitude for depression, with a consistently low read voltage of 1 mV, stimulation comprised a pulse with a constant width of 30 ms, and amplitudes were varied at (a) 0.3 V, (b) 0.4 V, (c) and 0.5 V.

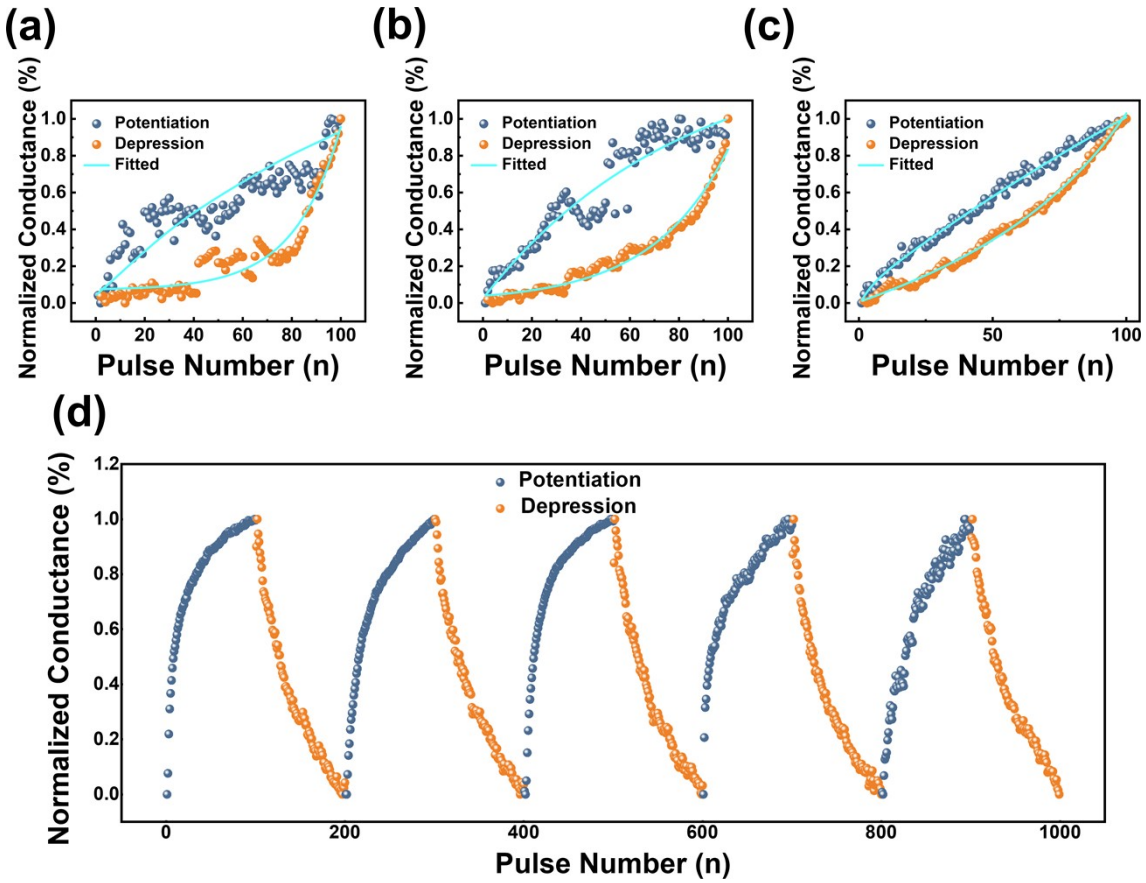

Fig S11. Non-linearity factor calculated using identical pulse methods for the artificial neural network (ANN), for (a) OM, (b) SM, and (c) OSM memristor devices respectively. (d) OSM Long-term plasticity of LTP and LTD stimulated by pulse train with varying pulse amplitude for 5 consecutive cycles

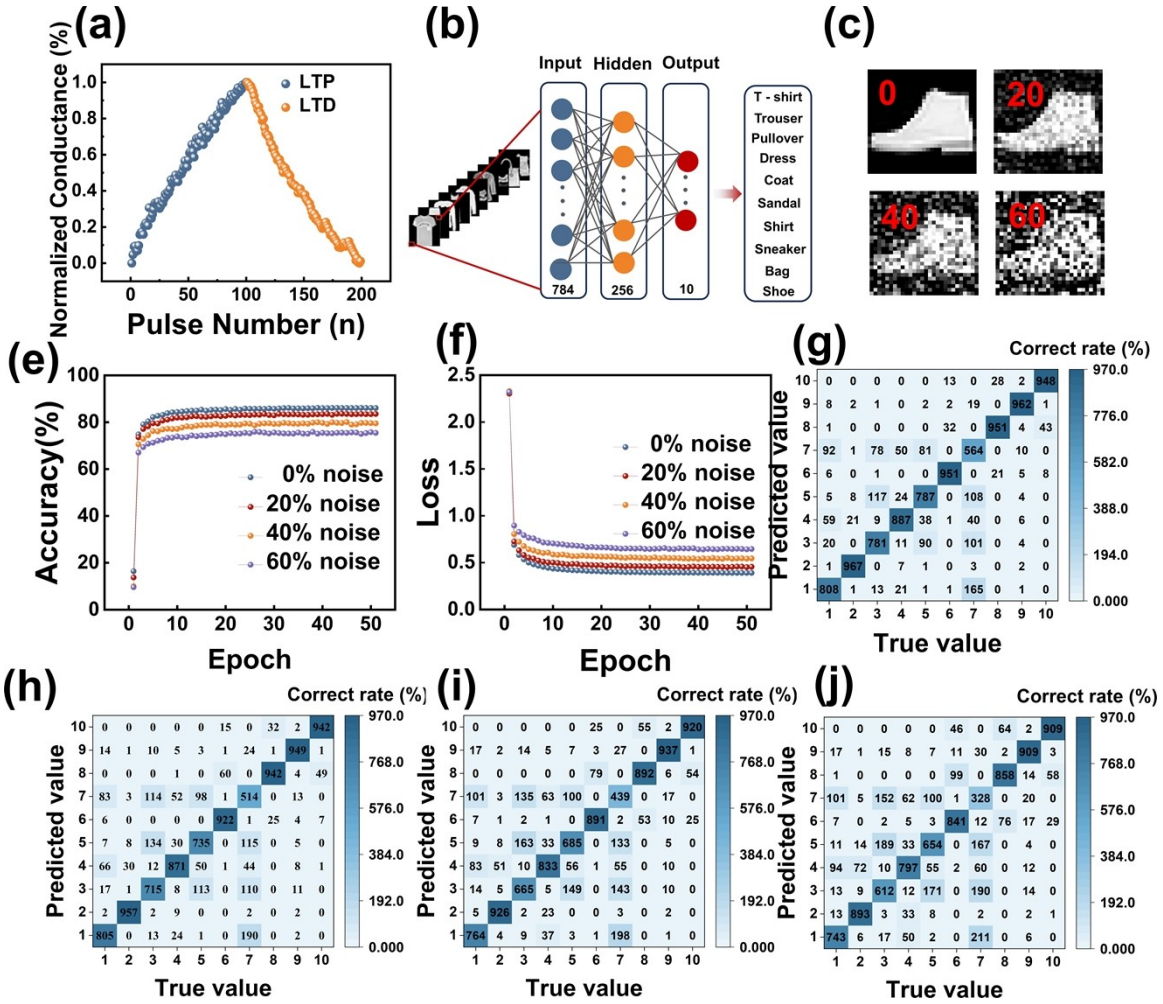

Fig S12. Potentiation/depression of OSMs at the 100 consecutive voltage pulse condition, (b) neural network diagram for digit recognition, (c) recognize output images under different noise; (d) recognition accuracy of the outfits “shoe” after 50 training sessions at 0%, 20%, 40%, and 60% noise; (e) the outfits “shoe” is loss after 50 training sessions at 0%, 20%, 40%, and 60% noise; confusion matrix for recognition of the outfits “shoe” in different noise cases: (f) 0%, (g) 20%, (h) 40%, and (i) 60%.

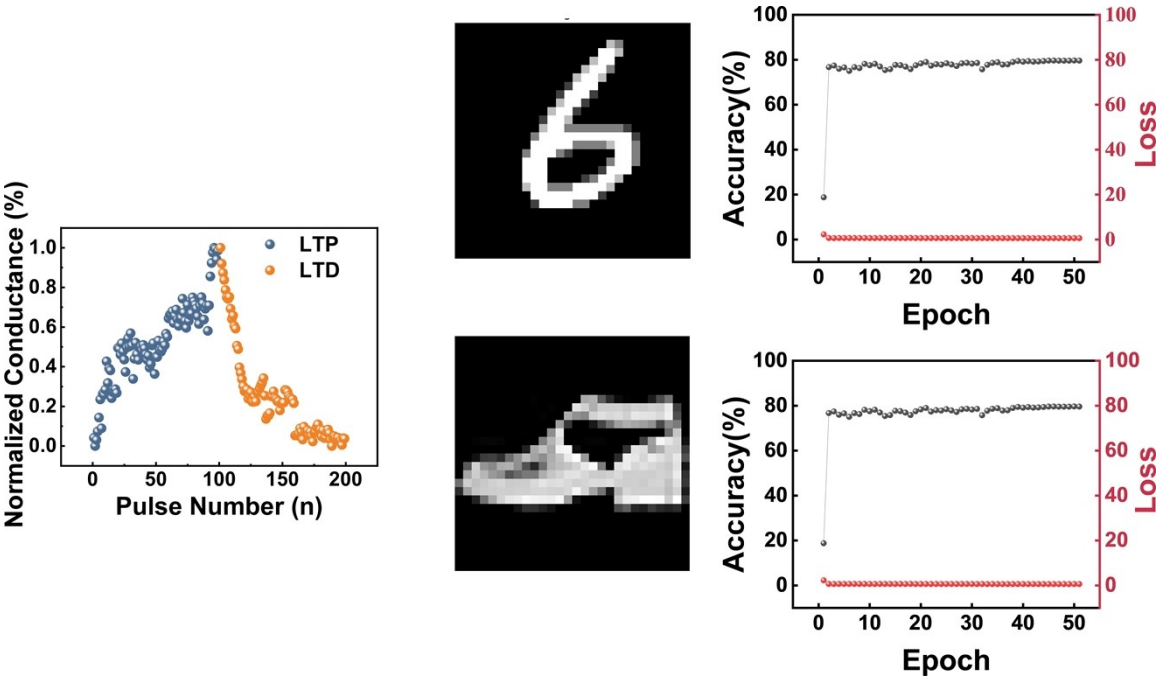

Fig S13. Simulation results for 28 × 28 digit and fashion MNIST classification using the LTP/LTD curves of OMs.

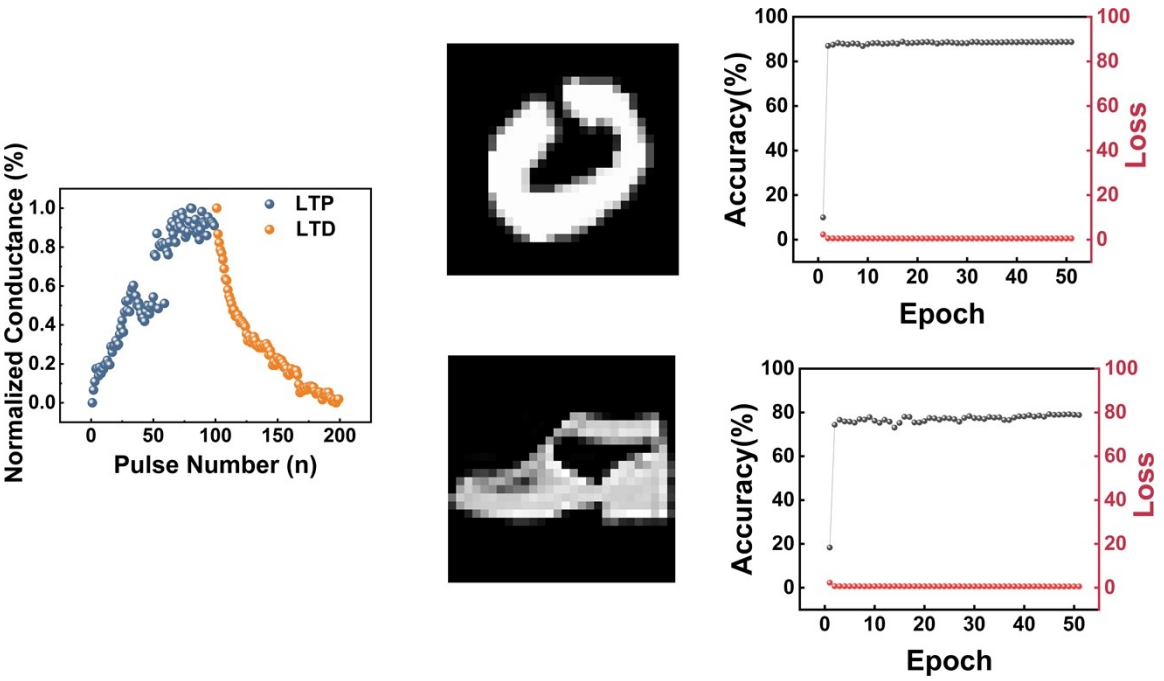

Fig S14. Simulation results for 28 × 28 digit and fashion MNIST classification using the LTP/LTD curves of SMs.

Additional scheme

Scheme S1. Schematic graphs of preparing process for depositing SnS_2 and SnO_2 thin films.

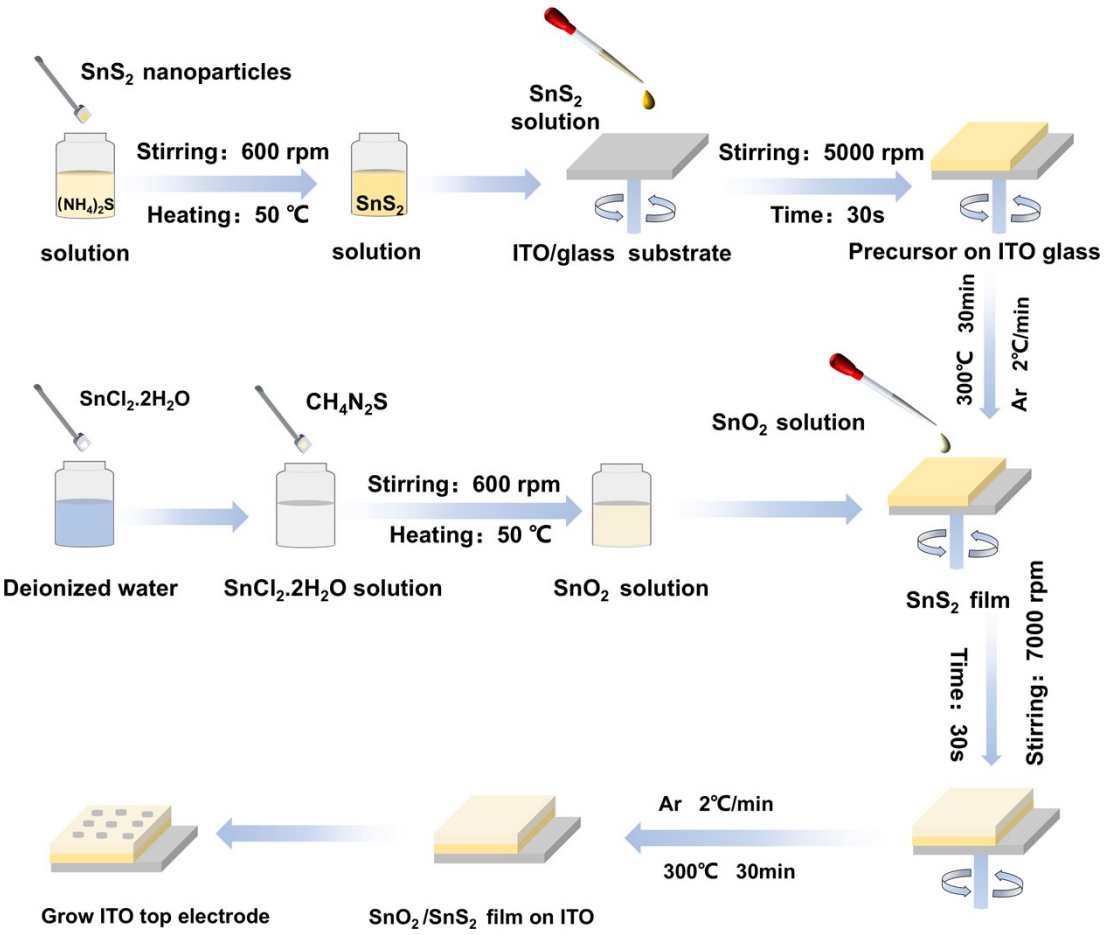

Additional tables

Table S1. Performance comparison with reported devices.

Device Structure	*On-off ratio*	*DC Endurance (cycles)*	*Retention (s)*	*Source*
ITO/SnS_2/ITO	5	800	10^4	[1]
Ag/SnO_2/FTO	5.4	100	1.4×10^3	[2]
Ag/ZrO_2/WS_2/Pt	> 10^2	——	4×10^4	[3]
W/SnO_2/ZTO/TIN	10	300	——	[4]
Ti/ZrO_2/SnO_2/ITO	> 10^2	120	——	[5]
Ag/$FAPbI_3$/SnO_2/ITO	> 10^2	1000	10^4	[6]
Ag/SnO_2/IGZO/Pt	> 10^2	——	10^4	[7]
ITO/SnO_2//ITO	> 10^2	200	10^4	This work
ITO/SnO_2/SnS_2/ITO	> 10^2	10000	10^4	This work

Table S2. Non-linearity factor calculated for identical pulse

Device Structure	*Potentiation*	*Depression*
ITO/SnO_2//ITO	11.20%	30.50%
ITO/SnS_2/ITO	13.40%	24.50%
ITO/SnO_2/SnS_2/ITO	3.30%	2.90%

References

1 J. Feng, J. Fan, Z. Zhang, Y. Gao, S. Xue, G. Cai and J. S. Zhao, *Adv. Funct. Mater.*, 2024, **34**, 2401228.

2 A. Kalateh, A. Jalali, M. J. Kamali Ashtiani, M. Mohammadimasoudi, H. Bastami and M. Mohseni, *Sci Rep*, 2023, **13**, 20036.

3 X. Yan, C. Qin, C. Lu, J. Zhao, R. Zhao, D. Ren, Z. Zhou, J. Wang, L. Zhang, X. Li, Y. Pei, G. Wang, Q. Zhao, Z. Xiao and H. Li, ACS Appl. Mater. Interfaces, 2019, **11**, 48029–48038.

4 M. K. Rahmani, M. Ismail, C. Mahata and S. Kim, *Results in Physics*, 2020, **18**, 103325.

5 K. Choi and J. J. Pak, *Semicond. Sci. Technol.*, 2024, **39**, 045012.

6 S.-U. Lee, S.-Y. Kim, J.-H. Lee, J. H. Baek, J.-W. Lee, H. W. Jang and N.-G. Park, *Nano Lett.*, 2024, acs.nanolett.4c00253.

7 A. Ali, Y. Abbas, H. Abbas, Y.-R. Jeon, S. Hussain, B. A. Naqvi, C. Choi and J. Jung, *Appl. Surf. Sci.*, 2020, **525**, 146390.